



# Study on the Characteristics of Vacuum-Bag-Only Processed Composites by Prepreg/Fiber Interleaved Layup

Yu-Yao Chang<sup>1</sup> · Wen-Bin Young<sup>1</sup>

Received: 29 August 2021 / Revised: 29 March 2022 / Accepted: 4 April 2022 / Published online: 13 February 2023  
© The Author(s), under exclusive licence to the Korean Fiber Society 2023

## Abstract

In this study, the vacuum-bag-only (VBO) process was used to fabricate composite laminates by employing interleaved unidirectional fully impregnated prepreg and dry fiber. The mechanical test results show that the flexure strength, compression after impact (CAI) strength and compression before impact (CBI) strength of the carbon fiber composite laminate produced by this process are about 84%, 72% and 83% of the autoclave composite laminate, respectively. The CAI strength with impact energy of 8.5 J retained about 85.4% and 96.4% of the original strength, respectively, for the components fabricated by the interleaved layup VBO and conventional autoclave processes. Ultrasonic scanning was performed for the 50×50 cm<sup>2</sup> unidirectional carbon fiber composite to identify the void distribution. The results show that the composites fabricated by interleaved layup VBO process have good quality and low porosity. In the case of glass fiber composites, the hybrid laminate of this process was used to fabricate composite laminate in which unidirectional glass fiber prepreps and bidirectional dry woven glass fiber fabric are interleaved layup. The ultrasonic test results show that the internal pores of this composite laminate are very few, and the quality is good. The feasibility of applying the process to different materials or woven materials was demonstrated.

**Keywords** Out-of-autoclave process · Vacuum-bag-only process · Prepreg/fiber · Bending test · CAI test

## 1 Introduction

Most high-performance structural composites for aerospace applications were made by the prepreps, which are layers of carbon fiber beds pre-impregnated with a catalyzed but uncured resin [1]. The prepreg layup process consists in stacking fully impregnated prepreg on a mold to form a laminate. Then, after covering it with some consumable materials and enclosed in a vacuum bag, the assembly is placed in an autoclave for heating (up to 180 °C) and consolidation (up to 10 atm). The high-pressure difference between the autoclave and the vacuum bag will compact the laminate and conform to the contour of the mold, driving the resin together with the bubbles between the laminate layers and/or the volatiles into the bleeders. The bleeding excess resin will be absorbed by bleeders to suppress pore content in the composite. Therefore, parts manufactured using the

autoclave process have excellent characteristics such as high mechanical properties, low porosity, and precise dimensions. However, despite the robustness of the autoclave process, this process has some disadvantages, such as high equipment and operating costs, slow production rates, non-cost-effective manufacturing of small parts, and the size limitation due to equipment capacity. Therefore, an alternative method that can provide compatible quality at a lower cost was later developed. One of the options is the out-of-autoclave (OOA) process [2, 3]. OOA is an alternative to the traditional high-pressure autoclave curing process used by the composite manufacturers. The curing and elimination of voids of OOA were achieved by applying vacuum, pressure, and heat by means other than an autoclave.

The vacuum-bag-only (VBO) process uses the vacuum bag for consolidation, where the equipment and operating costs are significantly reduced. Moreover, it has good manufacturing flexibility and can be matched with various heating equipment, such as traditional ovens, heating blankets or heating plates, which has a revolutionary impact on the industry [4]. However, since this processing method only applies the atmospheric pressure to compact the laminate,

✉ Wen-Bin Young  
youngwb@mail.ncku.edu.tw

<sup>1</sup> Department of Aeronautics and Astronautics, National Cheng Kung University, Tainan 70101, Taiwan

the air bubbles in the laminate cannot be eliminated effectively, and void defects are easily formed inside the laminate. To solve this problem, material manufacturers have developed two common methods to produce VBO prepregs (or OOA prepreg). The first method is to use perforated resin film, which can make the resin in the prepreg have gaps. The second method is to partially impregnate the fiber/woven fabric with resin to form a prepreg [5]. The partial penetration will leave dry fiber areas in the prepreg to form engineered vacuum channels (EVaC). During the consolidation process, these channels can help the gas flow in a direction parallel to the laminate to the edges of the prepregs. Using breather to connect the edges of the prepreg is the most common method to lead the air to the vacuum pipe in VBO laminate manufacturing [2, 4].

VBO prepreg materials have been developed for decades. The research of many scholars has proved that, as long as appropriate process parameters or processing methods were employed to make composite laminates, its quality and mechanical strength could reach those of autoclave-processed composite laminates. For example: Parker et al. [6] compared the characteristics of carbon fiber composite laminates made of traditional prepregs using the autoclave process and VBO prepregs in the OOA process. The research results showed that the content of the porosity and surface porosity of the composite laminate were relevant to the viscosity variation of the resin during the curing process. If the resin fluidity was adequate, high-quality composite laminates with low porosity (1.3%) and high fiber volume ratio (53vol.%) could be produced. In addition, the mechanical performance test results showed that the plane shear strength and compressive strength of the composite laminate could be compared with the traditional autoclave composite laminate. Hughes et al. [7] discussed the application of VBO prepreg

in the production of complex geometric shapes. The author used the traditional prepreg in the autoclave process and the VBO prepreg in the OOA process to make carbon fiber cabin doors, and analyzed the surface defects, porosity and geometry of the parts. The research results showed that the surface and geometric defect types of the two composite laminates were similar, and there were warpages and corner wrinkles. However, this is a problem that often arises when manufacturing parts with complex shapes. It can be improved by adjusting the mold design or other methods. The porosity of different contour parts tested by OOA composite parts is between 0.09 and 1.73%. Practice has proved that the OOA process can not only reduce the production costs, but also produce a quality similar to autoclave composite laminates.

However, since only a few material manufacturers in the industry have mastered the manufacturing technology of OOA prepregs, in view of the relatively expensive price and freight, long delivery time and possible minimum order quantity (MOQ) and other factors, it is inconvenient to get the materials. Therefore, it is desired that common and popular materials can be used in the OOA process and generate composites with similar quality.

In addition, schematic diagrams of the consolidation processes for different manufacturing processes are shown in Fig. 1. Diagram (A) shows the consolidation process of a traditional autoclave prepreg laminate. In the fully impregnated prepreg lamination process, air bubbles will be entrained between layers. During the consolidation process, the bubbles are crushed by the high-pressure difference between the autoclave and the vacuum bag. Simultaneously, as the temperature rises, the viscosity of the resin decreases, and the micro bubbles will flow to the surface of the laminate along with the excess resin and be absorbed by the bleeder and finally complete the curing. Diagram (B) shows the consolidation process

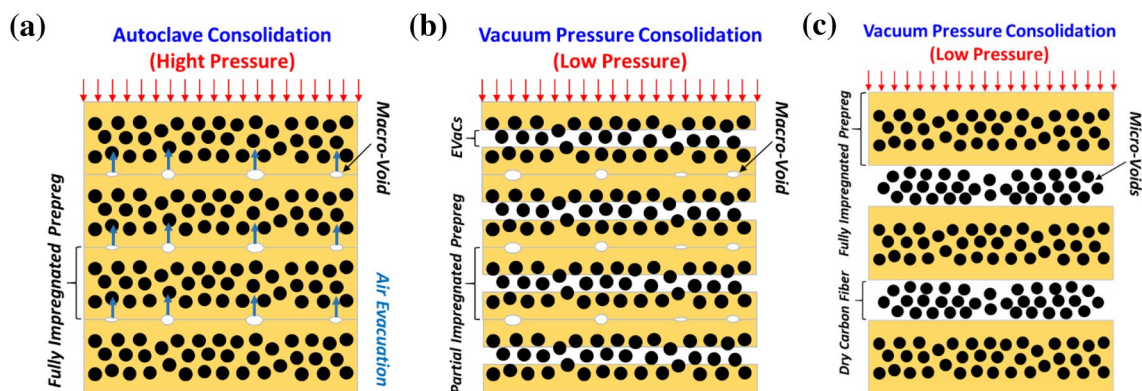


Fig. 1 Schematic of the three stages of consolidation vs temperature and laminate thickness [21]

of traditional VBO prepreg laminates. Partially impregnated prepreg also has the opportunity to entrap air bubbles between layers during the laminating process. During the consolidation process, the vacuum bag only applies 1 atm to compact the laminate. In the process of vacuuming at room temperature, the gas can be evacuated along the fiber direction by the EVaCs. After heating, the resin infiltrates the channel and completes curing. Diagram (C) is the process of using dry fiber fabric sandwiched in the fully impregnated prepreg. The exposed edge of the dry fiber fabric in the fiber direction is directly connected to the breather, and the dry fiber area is used as an exhaust channel to allow gas to flow and exhaust along the fiber direction. After heating, the resin of the prepreg will infiltrate the dry fiber fabric and finally finish curing.

Yang et al. [8] applied the VBO process to fabricate composite laminates in which fully impregnated prepreg and dry fiber fabric were interleaved layup for consolidation. The results of focus ion beam (FIB) micrographs and tensile testing confirmed that the composite laminate of this process had a low porosity and tensile strength similar to the composite laminate of the autoclave process. However, since this method was a newly developed process, there were still many performance, characteristics, and application challenges that had not been tested. Therefore, this study uses more representative tests to further study and discuss the process.

This study aimed to explore the uniformity of large-area composite laminates made by using interleaved layup of prepreg and dry fibers VBO process. Therefore,  $50 \times 50 \text{ cm}^2$  carbon fiber composite laminates were produced, and three experiments were carried out to explore the uniformity of their quality. First, ultrasonic flaw detection was performed on the composite laminate, and the distribution of pores in the composite laminate during this process was discussed. Next, measuring the thickness of the composite laminate at nine specific points was performed to explore the uniformity of the thickness distribution of the composite laminate. Then, the composite laminate was subjected to a three-point bending test to determine the uniformity of its flexure properties. To further understand the mechanical properties of the composite laminate in this process,  $30 \times 30 \text{ cm}^2$  composite laminates were made by this process and the autoclave process, respectively. The bending test, CAI test, and CBI test were conducted to discuss the strength difference of the composite laminates. Finally, micrographs of the specimen were taken by FIB to study the pore distribution inside the microstructure. In addition, this process was applied to the case of weaving fiber composite laminates, where the unidirectional glass fiber prepreg and bidirectional woven glass dry fiber fabric were used to make glass fiber composite laminate.

## 2 Experimental

### 2.1 Materials

The UD150 unidirectional carbon fiber prepreg and AD300 unidirectional dry carbon fiber fabric used in this study were both provided by Wah Hong Industrial Crop, Taiwan. UD150 unidirectional carbon fiber prepreg was composed of 37wt% epoxy resin and HTS40 carbon fabric by Toho Tenax Co., Ltd. AD300 unidirectional dry carbon fiber fabric is woven from 12 K carbon fiber warp yarns with hot-melt glass fiber yarns as weft yarns. Unidirectional glass fiber prepreg was supplied by Wah Hong Industrial Crop, Taiwan. It was composed of 35wt% epoxy resin and R1062 glass fiber by PFG Fiber Glass Co., Ltd. Bidirectional dry woven glass fiber fabric was supplied by Airtech International Inc. In this study, the single-layer prepreg was named  $P_a$ . To increase the resin content of the prepreg per unit area, two layers of prepreg were laminated and named  $P_b$ . The detailed specifications and images of the above materials are shown in Tables 1 and 2.


### 2.2 Manufacturing Procedure

In this study, a dry fiber fabric is sandwiched between the layers of the fully impregnated prepreg. Its function is similar to the EVaCs in the VBO prepreg, which can help to remove the interlayer air and the volatiles generated during the layup and heating processes. The fabrication of prepreg/fiber composite laminate uses the combination of [P/F/P/F/P], where P stands for unidirectional carbon fiber prepreg and F stands for unidirectional dry carbon fiber fabric. The consolidation of the laminate consists of three stages: fiber bed compaction, air evacuation, and resin flow. The three stages of consolidation are shown in Fig. 2, including the relationship between the thickness of the composite laminate and the temperature curve. The microstructures corresponding to each stage are shown in Fig. 3. During Stage I, the initial form of the laminate is shown in diagram (A) of Fig. 3. After being evacuated for a period of time at room temperature, the laminate is compressed by the vacuum bag. Part of the gas is exhausted from the vacuum source along the fiber direction of the dry fiber zone, so that the thickness of the laminate is reduced, as shown in diagram (B). At this time, the fiber volume ratio increases as the degree of compaction increases, while the porosity and permeability of the prepreg decrease. During Stage II, after the laminate is heated, the viscosity of the resin in the prepreg decreases as the temperature rises. The compaction of the vacuum bag drives the resin to infiltrate the dry fiber area and fill the pores until the laminate reaches a saturated state, as shown

**Table 1** Characteristic of the carbon fiber prepreg and dry carbon fiber [8]

	Carbon fiber prepreg $P_a$	Carbon fiber prepreg $P_b$	Dry carbon fabric F
Surface density ( $\text{g}/\text{cm}^2$ )	$D_{p_a} = 0.0241$	$D_{p_b} = 0.0482$	$D_{df} = 0.0318$
Prepreg density ( $\text{g}/\text{cm}^3$ )	$\rho_p = 1.48$	$\rho_p = 1.48$	–
Fiber density ( $\text{g}/\text{cm}^3$ )	$\rho_{pf} = 1.78$	$\rho_{pf} = 1.78$	$\rho_{df} = 1.81$
Resin content	$w_r = 0.37$	$w_r = 0.37$	–
Resin density ( $\text{g}/\text{cm}^3$ )	$\rho_r = 1.15$	$\rho_r = 1.15$	–
Uncompressed thickness (mm)	$h_{p_a} = 0.166$	$h_{p_b} = 0.332$	$h_{df} = 0.482$

carbon fiber prepreg




dry carbon fiber

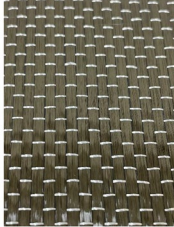


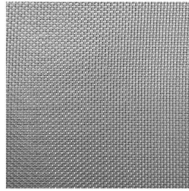
**Table 2** Characteristic of the glass fiber prepreg and dry glass fiber

	Glass fiber prepreg $P_a$	Glass fiber prepreg $P_b$	Dry glass fabric F
Surface density ( $\text{g}/\text{cm}^2$ )	$D_{p_a} = 0.0231$	$D_{p_b} = 0.0462$	$D_{df} = 0.0226$
Prepreg density ( $\text{g}/\text{cm}^3$ )	$\rho_p = 1.692$	$\rho_p = 1.692$	–
Fiber density ( $\text{g}/\text{cm}^3$ )	$\rho_{pf} = 2.54$	$\rho_{pf} = 2.54$	$\rho_{df} = 2.73$
Resin content	$w_r = 0.35$	$w_r = 0.35$	–
Resin density ( $\text{g}/\text{cm}^3$ )	$\rho_r = 1.04$	$\rho_r = 1.04$	–
Uncompressed thickness (mm)	$h_{p_a} = 0.1247$	$h_{p_b} = 0.2494$	$h_{df} = 0.2021$

glass fiber prepreg



dry glass fiber



in diagram (C). Finally, during Stage III, the resin is cured as the cross-linking reaction progresses, as shown in diagram (D).

This study made two different sizes of carbon fiber composites. One was of size  $50 \times 50 \text{ cm}^2$  and lamination  $[P_b/F/P_b]_2$ . The other was of size  $30 \times 30 \text{ cm}^2$  and lamination  $[P_b/F/P_b/F/P_b]_2$ ,  $[P_0/P_{90}/F_0/P_{90}/P_0/F_{90}/P_0/P_{90}]_5$  and  $[P_{90}/P_0/F_0/P_0/P_{90}/F_{90}/P_0/P_{90}]_5$ . One glass fiber composite was also fabricated with size  $20 \times 20 \text{ cm}^2$  and lamination  $[P_b/F/P_b/F/P_b]_2$ .

The procedures of the VBO method consist of four steps: ply cut, layup, debulking and cure. First, cut the material to the size corresponding to the composite laminate. The dimensions of prepreg/carbon fiber fabric required for

composite laminates of  $50 \times 50 \text{ cm}^2$  and  $30 \times 30 \text{ cm}^2$  are  $50 \times 50 \text{ cm}^2/50 \times 51 \text{ cm}^2$ , and  $30 \times 30 \text{ cm}^2/30 \times 31 \text{ cm}^2$ , respectively. The extra 1 cm of the dry fiber in the fiber direction will directly contact the breather to form a continuous air channel, so that the interlayer gas can be exhausted smoothly along this channel. Figure 4 shows the layout details of vacuum packaging. The resin-permeable Teflon layer can keep the surface of the composite laminate flat. The resin-impermeable release film can prevent the resin from flowing into the mold or breather. The breather must completely cover the composite laminates to distribute even compression pressure. In addition, the 2.00 mm depth in the mold cavity was used to prevent resin loss, so that the fiber

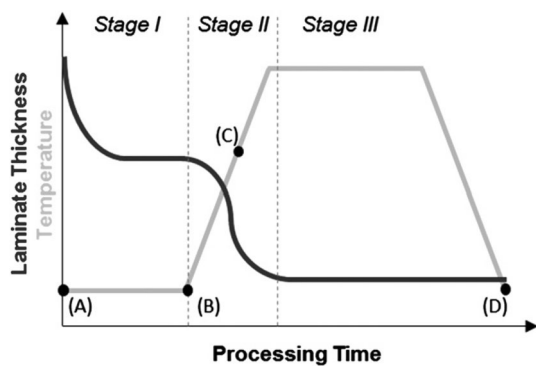


**Fig. 2** Schematic diagrams of the microstructure of the consolidation process of unidirectional carbon fiber/prepreg composite laminate (a) layup, (b) room temperature vacuum holding, (c) heated cure, and (d) post-cure

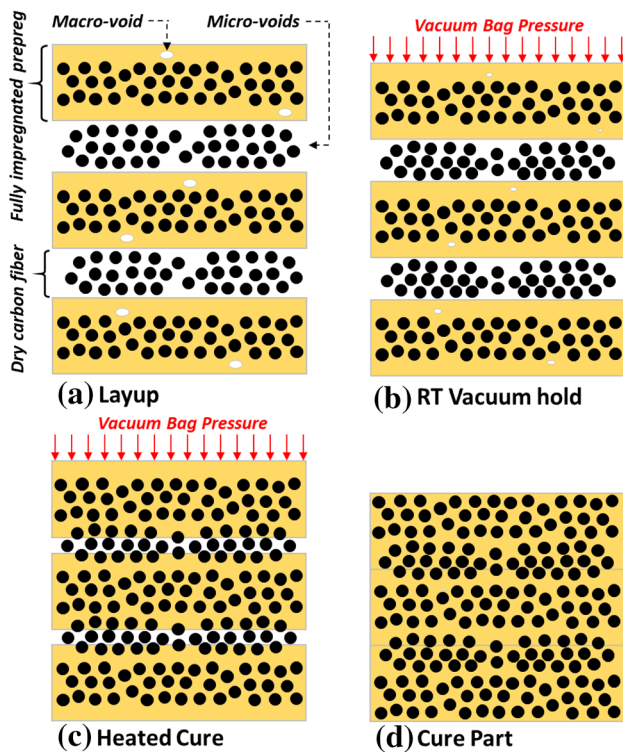


**Fig. 3** Schematic of the consolidation process of composite laminates of different manufacturing processes. (a) Traditional autoclave prepreg laminate, (b) traditional VBO prepreg laminate, and (c) OOA prepreg/dry fiber fabric composite laminate

volume ratio of the composite laminate could be accurately controlled.

After a vacuum bag was installed, a vacuum was applied at room temperature for 1 h. After that, the assembly was placed on a hot plate to heat the composite laminate to 120 °C for 2 h. As the temperature continued to rise, the

resin viscosity inside the composite laminate decreased. Simultaneously, the consolidation process would drive the resin to flow into the dry fiber area to complete the infiltration and fill the voids, and the cross-linking reaction was then carried out to achieve curing. Finally, the heating temperature was increased to 160 °C for 2 h. This step can promote the curing reaction degree and can also eliminate the internal stress of the laminate and improve the mechanical properties. Figure 5 is the temperature–pressure curve of the process.

### 2.3 Bending Test

The three-point bending test (or bending test) was widely used to test the flexural properties of the composite laminates. This test method can simultaneously determine the structural characteristics of the specimen in tension, compression, and out-of-plane shear. Therefore, it can reflect the influence of the internal pores of the composite laminate or the degree of bonding of the laminate interface [9].

A universal material testing machine (AG-250 kN, Shimadzu Corp, Japan) was used for bending test. The bending test was carried out according to the three-point test method specified in ASTM D790-17 [10]. Five specimens were tested to derive the average data for each composite laminate. The three-point bending test flexure is shown in Fig. 6. The thickness of the composite laminate in this study is 2.65 mm. According to the standard, the width of the test specimens is 12.70 mm. The span-to-depth ratio is 32:1. The overhanging distance is 20% of the span. The radii of the cross head and supports are  $5.0 \pm 0.1$  mm. The rate of cross-head motion is 4.50 mm/min. The bending test parameters are listed in Table 3. The positions of the bending test specimens cut from the  $50 \times 50$  cm<sup>2</sup> and  $30 \times 30$  cm<sup>2</sup> composite laminates are shown in Fig. 7(a) and (b), respectively. Before the test, specimens were dried at 80 °C for 2 h to remove the moisture. After the bending test, a dual-beam focused ion beam (FIB, FEI Nova-200 NanoLab Compatible) was used to analyze the failure section of each composite laminate.

The flexural strength ( $\sigma_F$ ) and modulus ( $E_F$ ) of the composite laminates were determined according to the following equations [10]:

$$\sigma_F = (3PL)/(2bd^2), \tag{1}$$

$$E_F = \frac{L^3m}{4bd^3}, \tag{2}$$

where  $P, L, b, d$  and  $m$  represent the flexural load, support span, width of specimen, depth of specimen, and the initial slope of the load–displacement curve (100–400N), respectively.

**Fig. 4** Exploded view of bagging components

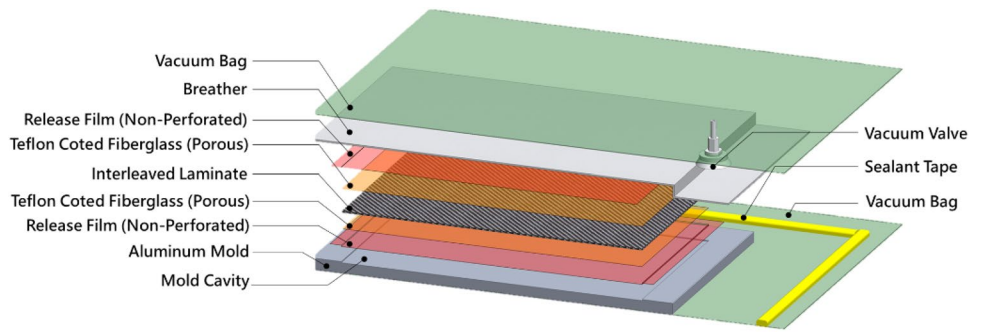


**Fig. 5** Schematic of the relationship between temperature and pressure in this process

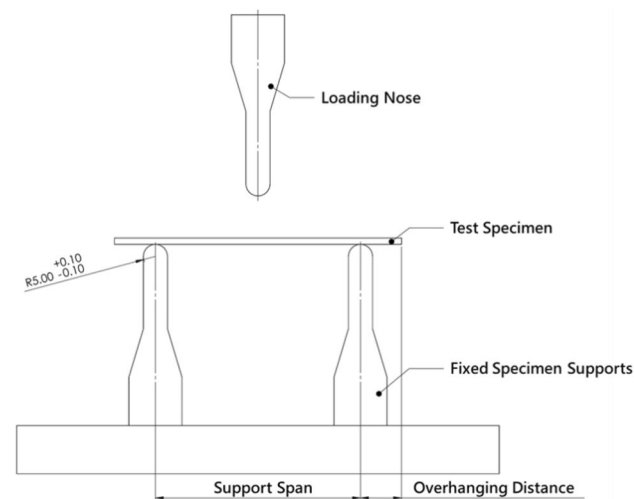
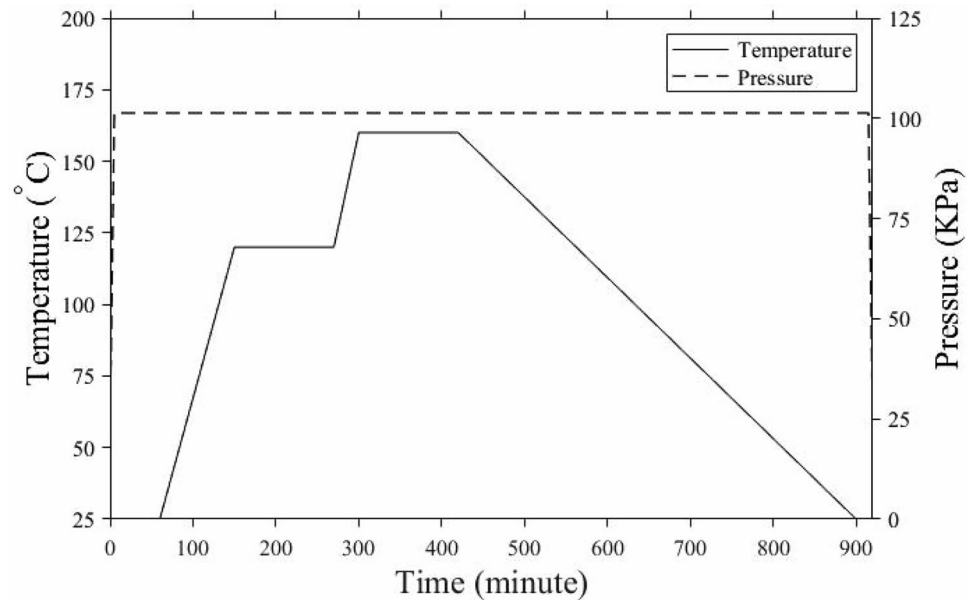


**Fig. 6** Schematic of three-point bending test method

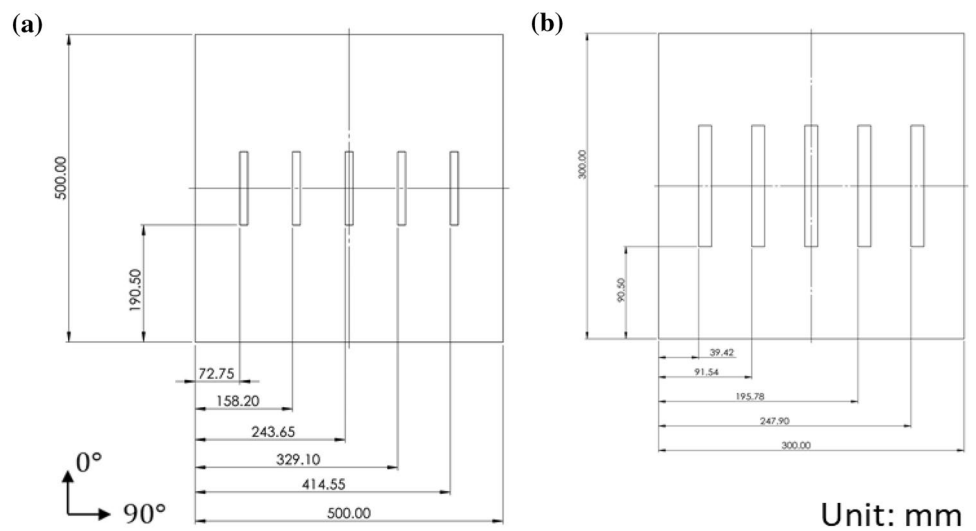
**Table 3** Experimental parameters of the three-point bending test method

	Parameter
Support span-to-depth ratio	32:1
Specimen thickness (mm)	2.65
Specimen wide (mm)	12.70
Overhanging distance (mm)	17.00
Support span length (mm)	85.00
Specimen total length (mm)	119.00
Rate of crosshead motion (mm/min)	4.500

### 2.4 Compression After Impact Methodology

Most composites are brittle so that they can only absorb energy in elastic deformation and through damage mechanisms, but not via plastic deformation. In addition, the composite laminate has superior performance only in the fiber

**Fig. 7** The position of the bending test specimen on the (a) 50×50 cm<sup>2</sup> composite laminate and (b) 30×30 cm<sup>2</sup> composite laminate



direction. Due to the lack of reinforcement in the thickness direction, the delamination and layer-to-layer load resistance is particularly poor [11]. Therefore, the composite laminate is very sensitive to damage caused by impact. In terms of inspection, damage caused by high-speed impact is not difficult to detect, because it is easy to be observed through visual inspection. However, this is not the case for low-velocity impact conditions. In this case, the composite laminate can pass through the local failure mechanism without large-scale plastic deformation. Hence, the impact load might cause a large amount of delamination and cracking of the matrix inside the laminate, which could not be sensed

on the surface. This kind of imperceptible injury is the most dangerous case [12]. According to research, the residual compressive strength of composite after impact (CAI) may only be 40–60% of that before impact [13]. Therefore, the ability to withstand impact loads is one of the important considerations in the design of aerospace composite material layered structures. This test refers to the ASTM D7136-15 [14] and D7137-17 standards [15] for low-speed impact test and CAI test. The CAI data of this study took an average of two test specimens for each composite laminate. The dimension of specimens and the position of the specimens cut from the composite laminate are shown in Fig. 8(a) and

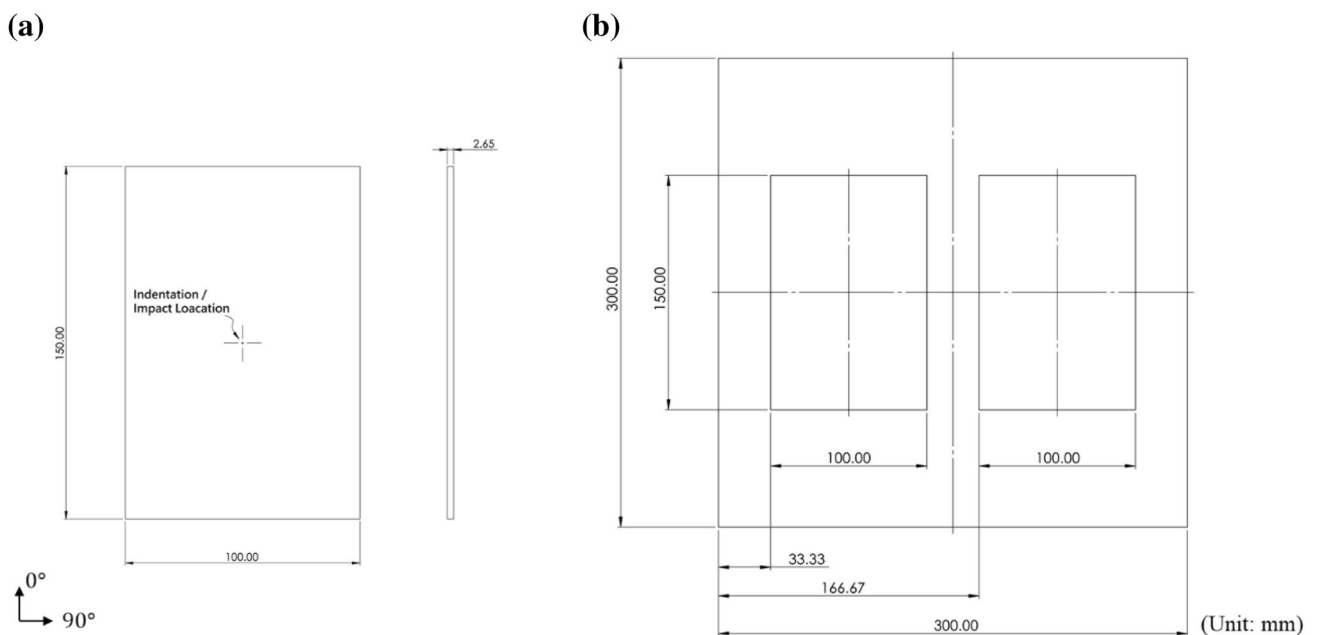
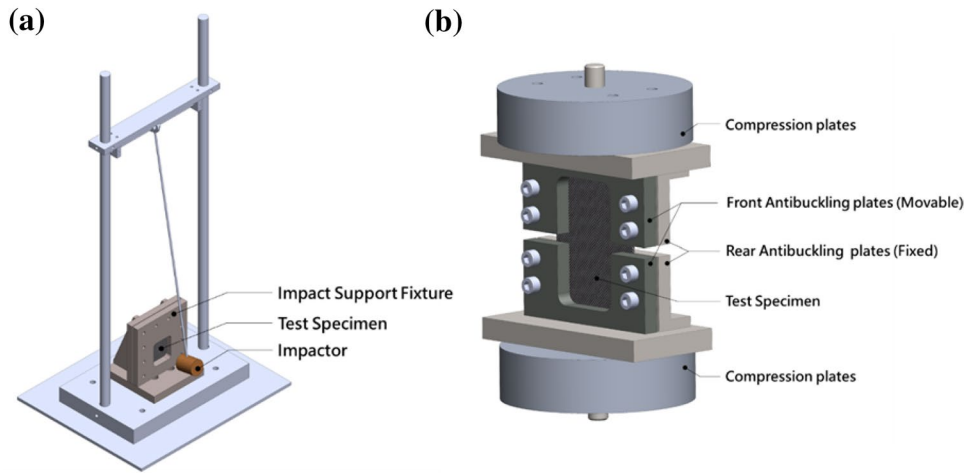


**Fig. 8** CAI/CBI test (a) dimension of specimens and (b) the position of the specimens on the composite laminate

**Fig. 9** CAI test (a) low velocity test device and (b) compression test device



(b) respectively. The pendulum-type low-velocity impact test device is shown in Fig. 9(a). The dimension of the clamp plates is 200 × 200 mm and the center has an opening of 70 × 80 mm. The specimen was placed in the setup against the clamp plates that was fastened to the rear plates by ten hand-tightened screws. The impactor in a horizontal position can apply an impact energy about 8.5 J to the composite laminate.

The CAI test fixture refers to the design of Sanchez-Saez [13] for testing as shown in Fig. 9(b). To prevent the impact surface of the test specimen from being affected, there is a rectangular opening in the center of the clamp plates on both sides of the test fixture. The dimension of the upper and lower anti-buckling plates is 70 × 160 mm and the central opening is 70 × 55 mm (both are upper and lower symmetrical). The crosshead displacement rate is 1.25 mm/min. In addition, we also conduct compression before impact (CBI) testing. The purpose is to determine the ultimate compressive strength that the composite laminate can withstand without impact damage.

For the CAI test, the ultimate compressive residual strength  $F^{CAI}$  and effective modulus  $E^{CAI}$  of the composite laminates were determined according to the following equations [16]:

$$F^{CAI} = P_{max}/A, \tag{3}$$

$$E^{CAI} = (P_{3000} - P_{1000}) / (\epsilon_{3000} - \epsilon_{1000}) \cdot A, \tag{4}$$

where  $P_{max}$ ,  $A$ ,  $P_{3000}$ ,  $P_{1000}$ ,  $\epsilon_{3000}$  and  $\epsilon_{1000}$  represent the maximum force prior to failure, cross-sectional area, applied force corresponding to  $\epsilon_{3000}$ , applied force corresponding to  $\epsilon_{1000}$ , recorded strain value closet to 3000 microstrain, and recorded strain value closet to 1000 microstrain, respectively.

### 2.5 Composite Panel Uniformity

To detect the uniformity of the composite laminate produced by this process, we will carry out ultrasonic inspection and thickness measurement of two  $[P_b/F/P_b/F/P_b]_2-50 \times 50 \text{ cm}^2$  composite laminates (one is identified as Laminate A and the other as Laminate B) as a check of repeatability. In this part, the Aeronautical Systems Research Division of National Chung-Shan Institute of Science and Technology (NCSIST) in Taiwan was commissioned to carry out ultrasonic testing. The ultrasonic waves with a frequency of 1 MHz are emitted by the transducer and transmitted through the water medium to the object. The reflected back signal was received by the same transducer. The attenuation or decrease of ultrasonic energy caused by the internal defects of the inspected object

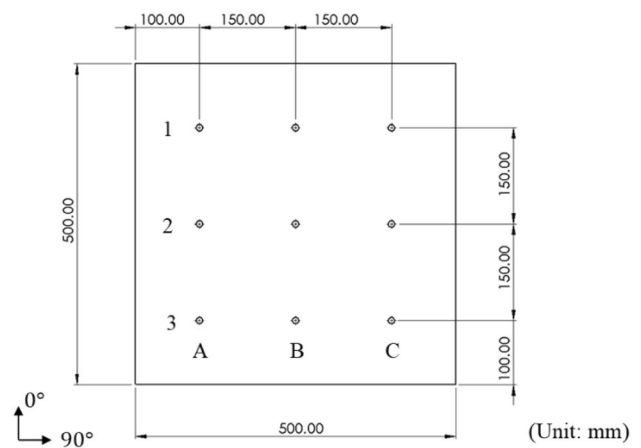


**Fig. 10** Thickness measurement positions in 50 × 50 cm<sup>2</sup> size composite laminate



was measured, so as to obtain the overall pore distribution of the composite laminate. The thickness uniformity test is measured by a micrometer (Mitutoyo, model: 103–137). The nine positions for measuring the thickness of the composite laminates are shown in Fig. 10.

### 2.6 Woven Glass Fiber Composites

To understand the application of this process to the production of woven fiber composite laminates, we used unidirectional glass fiber prepreg and bidirectional dry woven glass fiber fabric to produce glass fiber composite laminate. The design and production method adopted the experimental method proposed by Yang et al. [8]. First, measure the surface density, fiber density and resin density of the two materials. Next, to ensure that the pores of the fiber can be filled with resin under vacuum pressure, the fiber compression experiment is required to measure the fiber thickness of the material under different pressures. By calculating the material pressure–fiber thickness fitting equation, the combination of oversaturated glass fiber composite laminates can be designed. After the composite laminate was made, we also commissioned NCSIST to use an air-coupled ultrasonic scanner to perform ultrasonic inspection by the transmission inspection method. The transmitting transducer and the receiving transducer are, respectively, located on both sides of the side object, the axes of the two transducers are coincident, and they move synchronously for detection. The 250 kHz ultrasonic wave was transmitted through the laminate by the transmitting transducer and then received by the receiving transducer. The energy attenuation or decrease

caused by the internal defects of the composite laminate is measured to obtain the overall pore distribution of the composite laminate.

## 3 Results and Discussion

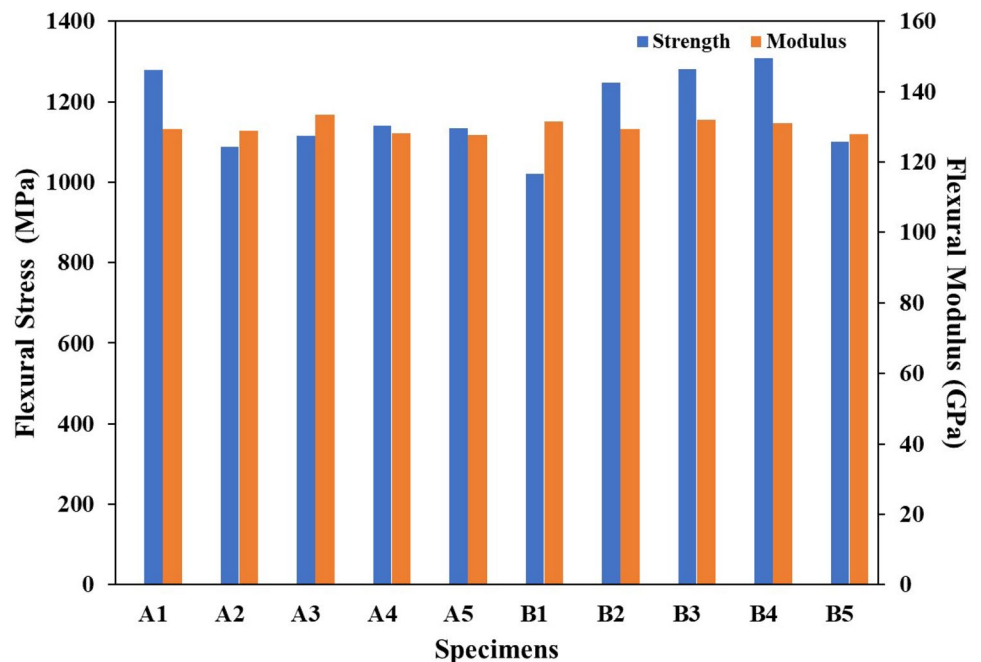
### 3.1 Bending Properties

The flexure strength and modulus of two  $[P_b/F/P_b/F/P_b]_2-50 \times 50 \text{ cm}^2$  composite laminates are shown in Fig. 11. The positions numbered 1–5 in the figure correspond to the specimens of the composite laminate from left to right in Fig. 7(a). The maximum flexural strength of the Laminate A specimen is 1279.67 MPa at the A1 position, and the minimum flexural strength is 1086.79 MPa at the A2 position. The maximum flexural strength of the Laminate B specimen is 1308.28 MPa at the B4 position, and the minimum flexural strength is 1020.25 MPa at the B1 position. Comparison of the two composite laminates shows that there is no obvious

**Table 4** Statistical results of bending test of the  $[P_b/F/P_b/F/P_b]_2-50 \times 50 \text{ cm}^2$  carbon fiber composite laminates

		Flexural strength, $\sigma_{fM}(MPa)$	Flexural modulus, $E_B(GPa)$
Laminate A	Average	1151.13 <sup>+128.54</sup> <sub>-64.34</sub>	129.51 <sup>+3.97</sup> <sub>-1.76</sub>
	SD	74.80	2.30
Laminate B	Average	1191.32 <sup>+116.96</sup> <sub>-171.07</sub>	130.34 <sup>+1.72</sup> <sub>-2.53</sub>
	SD	124.72	1.76

**Fig. 11** Histogram of flexure strength and modulus of the  $[P_b/F/P_b/F/P_b]_2-50 \times 50 \text{ cm}^2$  carbon fiber composite laminates



dependence of the position on the flexural strength. The average flexure properties of the two composite laminates are shown in Table 4. The average flexural strength of Laminate A composite laminate is 1151.13 MPa with the standard deviation of 74.80 MPa, and the average flexural modulus is 129.51 GPa with a standard deviation of 2.30 GPa. The average flexural strength of Laminate B composite laminate is 1191.32 MPa with the standard deviation of 124.72 MPa, and the average flexural modulus is 130.34 GPa with the standard deviation of 1.76 GPa. For the flexure strength and modulus, the average values of the two composite laminates are quite close. It can be confirmed that the application of this process to produce large-size composite laminates has good uniformity and reproducibility in terms of flexure strength. For the earlier investigations by Stamopoulos et al. [16], within the same stacking sequence and layers, their result showed the flexural strength of about 1250 MPa, which illustrated similar bending properties. Moreover, the flexural strength by interleaved layup was higher than that of other different process conditions. Mujahid et al. [17] and Pishvar et al. [18] carried out the modify cure cycle and magnet-assisted autoclave process, respectively, and showed the flexural strength to be around 800–900 MPa.

To compare with composite laminates fabricated by the interleaved prepreg/dry fiber VBO process, we also made  $[P_b/F/P_b/F/P_b]_2-30 \times 30 \text{ cm}^2$  composite laminates by the autoclave process. The average flexural strength of the five specimens is 1192.59 MPa, and the standard deviation is 84.38 MPa, which is very close to the result of the  $50 \times 50 \text{ cm}^2$  composite laminates. This once again reflects the high reproducibility of the process. The bending test data of  $[P_b/F/P_b/F/P_b]_2$  and autoclave ( $v_f = 0.65$ ) composite laminates are shown in Table 5. From the bending test results of the two composite laminates, the flexure strength of this process is about 15.7% lower than that of the autoclave process composite laminates. From this result, it can be seen that the flexure strength of the composite laminate of this process is lower than that of the autoclave composite laminate.

In terms of bidirectional laminated composite laminates, the results of the bending test of  $[P_0/P_{90}/F_0/P_{90}/P_0/F_{90}/P_0/P_{90}]_S$  and  $[P_{90}/P_0/F_0/P_0/P_{90}/F_{90}/P_{90}/P_0]_S$  carbon fiber composite laminates are shown in Table 6. The average flexural strength and flexural modulus of  $[P_0/P_{90}/F_0/P_{90}/P_0/F_{90}/P_0/P_{90}]_S$  composite laminate are about 897 MPa (SD is 50 MPa)

**Table 5** Comparison of bending test data of the  $[P_b/F/P_b/F/P_b]_2$  and autoclave process carbon fiber composite laminates

	Flexural strength, $\sigma_{fM}$ (MPa)	Flexural modulus, $E_B$ (GPa)
OOA – $[P_b/F/P_b/F/P_b]_2$	1192.59	126.21
autoclave ( $v_f = 0.65$ )	1414.89	122.64

**Table 6** Comparison of bending test data of the  $[P_0/P_{90}/F_0/P_{90}/P_0/F_{90}/P_0/P_{90}]_S$  and  $[P_{90}/P_0/F_0/P_0/P_{90}/F_{90}/P_{90}/P_0]_S$  carbon fiber composite laminates

	Flexural strength, $\sigma_{fM}$ (MPa)	Flexural modulus, $E_B$ (GPa)
$\{P_0/P_{90}/F_0/P_{90}/P_0/F_{90}/P_0/P_{90}\}_S$	896.78	81.15
$\{P_{90}/P_0/F_0/P_0/P_{90}/F_{90}/P_{90}/P_0\}_S$	1058.58	77.52

and 81 GPa (SD is 1.15 GPa), respectively. The average flexural strength and flexural modulus of  $[P_{90}/P_0/F_0/P_0/P_{90}/F_{90}/P_{90}/P_0]_S$  composite laminate are about 1059 MPa (SD is 34 MPa) and 78 GPa (SD is 0.59 GPa), respectively. Compared with the  $[P_{90}/P_0/F_0/P_0/P_{90}/F_{90}/P_{90}/P_0]_S$  carbon fiber composite laminate, the flexure strength of  $[P_0/P_{90}/F_0/P_{90}/P_0/F_{90}/P_0/P_{90}]_S$  is increased by about 18%. It can be seen that the lamination sequence has some effect on the flexure strength, and the following microstructure analysis will explain the reason.

### 3.2 Microscopic Analysis

The FIB micrograph of the cross section of  $[P_b/F/P_b/F/P_b]_2$  carbon fiber composite laminate is shown in Fig. 12. In Fig. 12(a), the fibers are well impregnated with resin. Figure 12(b) shows the magnification image of the  $[P_b/F]$  interface region. The top layer in the picture is the prepreg ( $P_b$ ), and the bottom layer is the dry fiber (F). The middle part shows the weft binding yarn of the dry fiber fabric. Since the directions of the weft binding yarn and the carbon fiber yarn are different, there exists a gap between the wavy weft yarn and the carbon fibers. This results in a tendency for resin to accumulate at the junction gap, leading to a resin-rich area.

Figure 13(a) shows the fractured surface of the specimen at the compressive side under the bending test. The fracture surface is quite smooth with no obvious fiber pullout. Figure 13(b) shows the fracture surface of the specimen at tensile side under the bending test. The fiber fracture surface appears irregular, and some fiber pullout can be noticed. In these two pictures, we can clearly observe the holes formed after the fiber breaks by pulled out, and the separation of resin and fiber filaments. Figure 14(a) shows the magnification image of the  $[F/P_b]$  interface region. Some separation appears inside the weft binding yarn, but the overall adhesion between the carbon fiber and the binding yarn remains intact. Figure 14(b) is the side view at the compression side after the bending test. There is obvious delamination in many places and buckling of the fibers at the crack area.

The micrographs of the  $[P_0/P_{90}/F_0/P_{90}/P_0/F_{90}/P_0/P_{90}]_S$  carbon fiber composite laminate were also taken. Figure 15(a) shows the cross section of the bidirectional composite. It can be clearly observed that the interface at the  $[P_{90}/F_0/P_{90}]$  area

**Fig. 12** Cross-sectional micrographs of the (a)  $[P_b/F/P_b/F/P_b]_2$  carbon fiber composite laminate and (b)  $[P_b/F]$  interface region

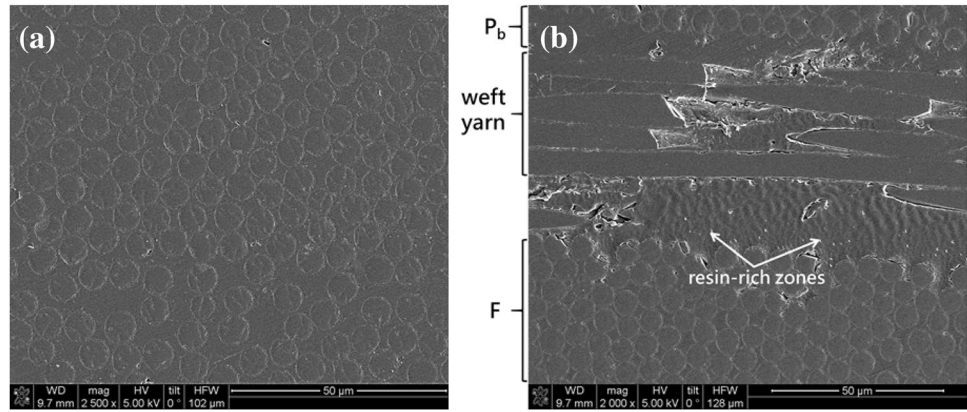


**Fig. 13** Cross-sectional micrographs of the fractured surfaces of the  $[P_b/F/P_b/F/P_b]_2$  carbon fiber composite laminate after flexural loading: (a) compression side and (b) tension side

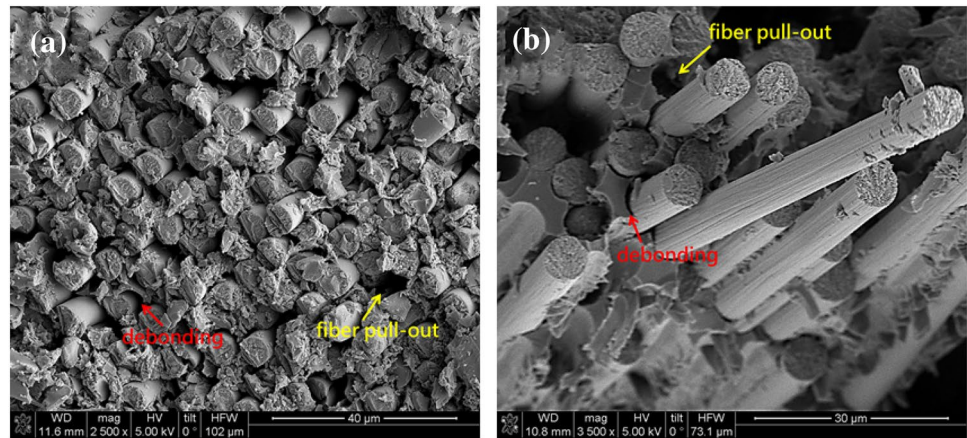
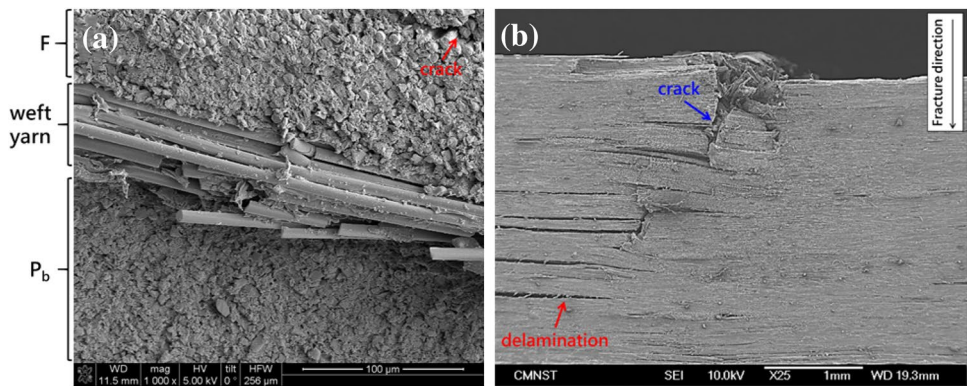


**Fig. 14** FIB micrographs of the fractured surfaces of the  $[P_b/F/P_b/F/P_b]_2$  carbon fiber composite laminate after flexural loading: (a) cross section of the  $[F/P_b]$  interface region and (b) side view at the compression side



has obvious defects. Figure 15(b) shows the magnification image of this defect. The carbon fiber tows of  $F_0$  form gaps due to the wavy weft yarn. Because the fiber directions of the dry fabric and prepregs ( $P_{90}$ ) are different, it is difficult to fill the gaps in the resin and fiber from the prepreg, which results in the formation of void defects. Figure 16(a) shows the schematic diagram of the  $[P_{90}/F_0/P_{90}]$  area. By adjusting the transparency of  $P_{90}$ , the weft yarn position of the carbon fiber dry fabric can be clearly seen. Figure 16(b) shows the right side view of the area. Since the carbon fiber filaments

of the prepreg cannot fill the gaps between the carbon fiber of the dry fabric tows, a void similar to an “hourglass” shape was formed. This defect results in the composite laminate containing voids inside. Therefore, it is easy to cause damage from this position when subjected to external load, resulting in a decrease in overall strength. Figure 17(a) is the cross-sectional micrograph of the specimen after the bending test. It clearly shows the delamination at the interface of  $F_0$  and  $P_{90}$ . Figure 17(b) shows the magnification image of the  $[P_{90}/F_0/P_{90}]$  area. The weft yarn of the dry carbon fiber

**Fig. 15** Cross-sectional micrographs of the (a)  $[P_0/P_{90}/F_0/P_{90}/F_0/P_{90}/P_0/P_{90}]_S$  carbon fiber composite laminate and (b)  $[P_{90}/F_0/P_{90}]$  area

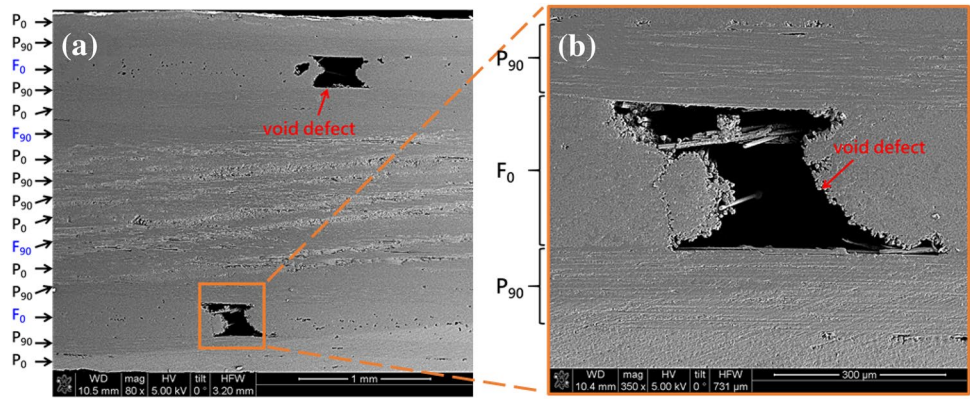


**Fig. 16** Schematic of the microstructure of the  $[P_{90}/F_0/P_{90}]$  area of the  $[P_0/P_{90}/F_0/P_{90}/P_0/P_{90}/F_0/P_{90}/P_0/P_{90}]_S$  carbon fiber composite laminate: (a) isometric view and (b) right side view

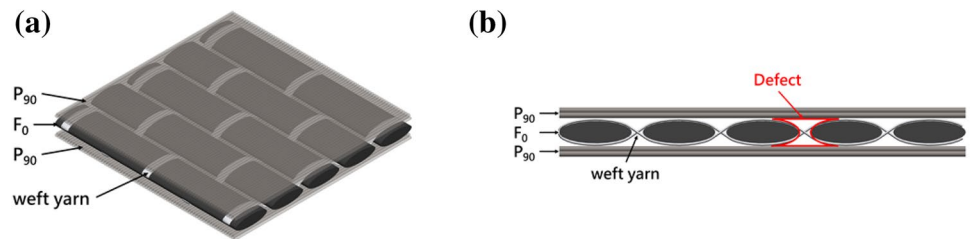


**Fig. 17** Cross-sectional micrographs of the fractured surfaces of the  $[P_0/P_{90}/F_0/P_{90}/P_0/P_{90}/F_0/P_{90}/P_0/P_{90}]_S$  carbon fiber composite laminate after flexural loading and (b)  $[P_{90}/F_0/P_{90}]$  area

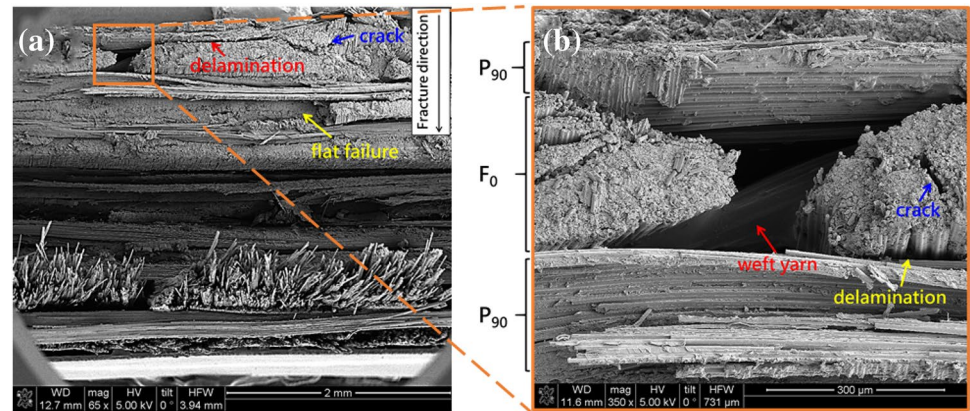


**Fig. 18** Cross-sectional micrographs of the fractured surfaces of the  $[P_0/P_{90}/F_0/P_{90}/P_0/P_{90}/F_0/P_{90}/P_0/P_{90}]_S$  carbon fiber composite laminate after flexural loading: (a) compression side and (b) tension side

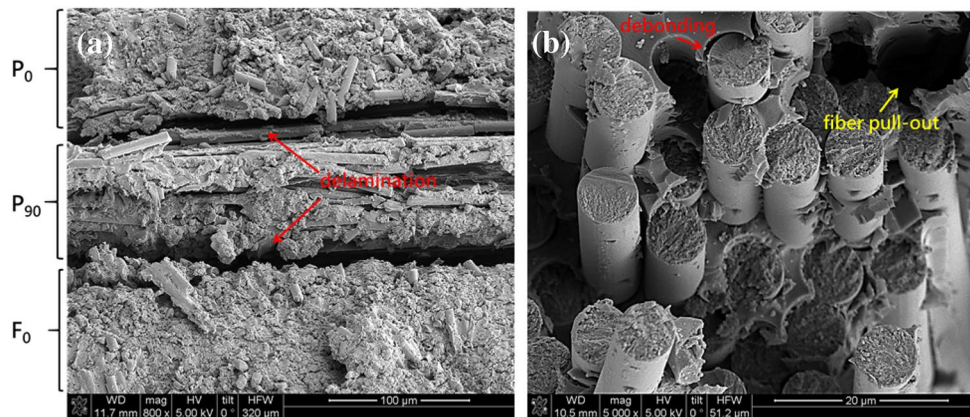


**Fig. 19** Cross-sectional micrographs of the (a)  $[P_{90}/P_0/F_0/P_0/P_0/F_{90}/P_{90}/P_0]_S$  carbon fiber composite laminate and (b)  $[P_{90}/F_{90}]$  area

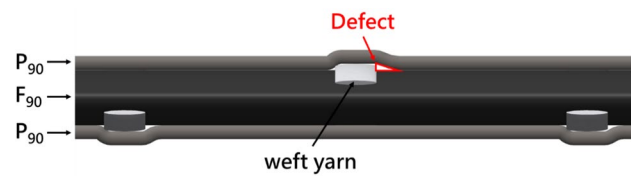
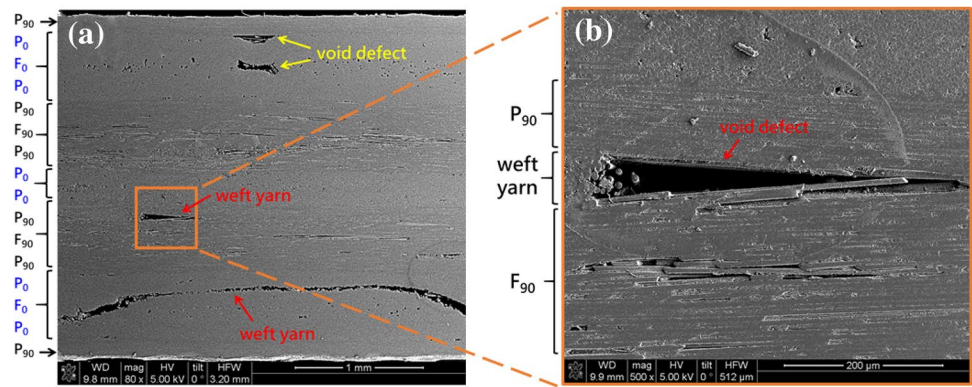


**Fig. 20** Schematic of the cross-sectional microstructure of the  $[P_{90}/F_{90}/P_{90}]$  area of the  $[P_{90}/P_0/F_0/P_0/P_0/F_{90}/P_{90}/P_0]_S$  carbon fiber composite laminate

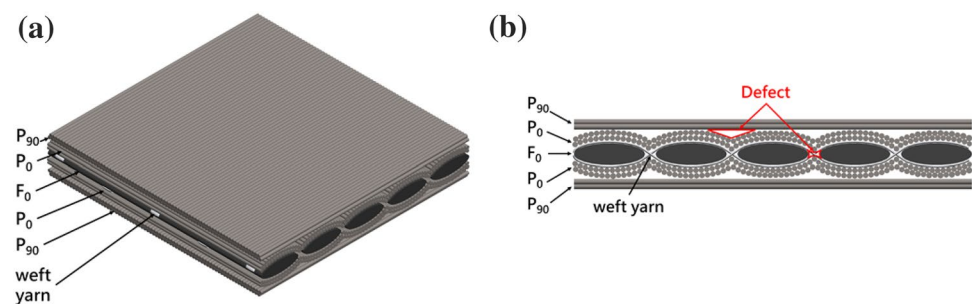
fabric can be observed, and there is no resin in the hour-glass voids. Figure 18(a) shows the fracture surface of the specimen under compressive stress. It can be observed that delamination occurs at the junction where the fiber direction is different, and Fig. 18(b) shows the result of the fracture surface subjected to tensile stress.

For the  $[P_{90}/P_0/F_0/P_0/P_0/F_{90}/P_{90}/P_0]_S$  carbon fiber composite laminate, Fig. 19(a) shows the cross section of the specimen. First, we can see that there is a void defect at the junction of  $[P_{90}/F_{90}]$ . Figure 19(b) shows the magnification image of this area. In this layup sequence, the adjacent layers of dry fabric and prepreg have the same fiber directions. When the  $P_{90}$  fiber is in contact with the  $F_{90}$  weft yarn, the fiber filaments of the prepreg will bulge and cannot completely adhere to the dry carbon fiber fabric. As a

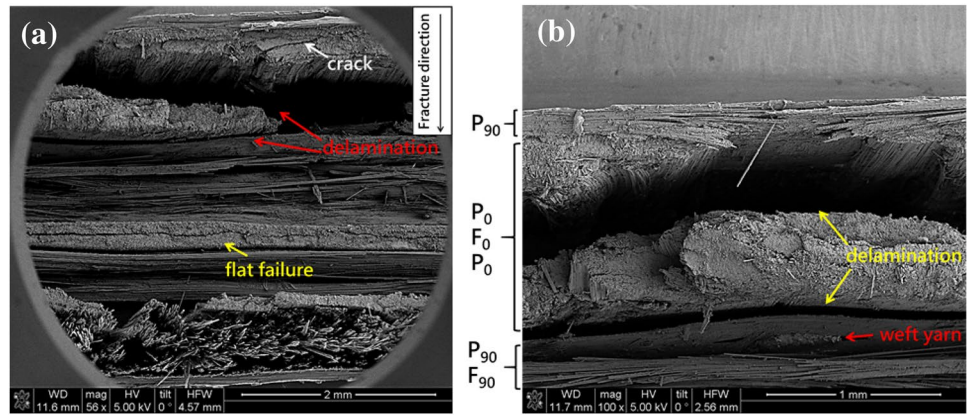
result, a small triangular void defect was formed. Figure 20 shows the schematic of the  $[P_{90}/F_{90}/P_{90}]$  area, it can clearly explain this phenomenon. In addition, in Fig. 19(a), it can also be observed that although the  $[P_{90}/P_0/F_0/P_0/P_0/P_{90}]$  area has improved the void defects in the  $[P_0/P_{90}/F_0/P_{90}/P_0]$  area in Fig. 15, it still has random gaps between the carbon fiber tows. Figure 21(a) shows the schematic isometric view of the microstructure of the  $[P_{90}/P_0/F_0/P_0/P_0/P_{90}]$  area, and (b) is the right side view. The  $P_0$  carbon fiber filaments fill the gaps between the dry carbon fiber tows, but there is still a probability to form tiny pores at the position of the weft yarn. Therefore, the fiber sags at this position, resulting in the formation of pores at the junction of  $P_{90}$  and  $P_0$ .

Figure 22(a) is the cross-sectional view of the specimen after the bending test. Figure 22(b) shows the magnification image of  $[P_{90}/P_0/F_0/P_0/P_0/P_{90}/F_{90}]$  area. It can be observed that the shape of the  $0^\circ$  fiber area where delamination occurs is consistent with the path of the dry carbon fiber fabric weft yarn, and delamination also occurs at the junction of  $P_0$  and  $P_{90}$ . Therefore, it can be determined that this laminated combination has weaker strength at the junction of the weft yarns, and delamination is prone to occur.

**Fig. 21** Schematic of the microstructure of the  $[P_{90}/P_0/F_0/P_0/P_0/P_{90}]$  area of the  $[P_{90}/P_0/F_0/P_0/P_0/F_{90}/P_{90}/P_0]_S$  carbon fiber composite laminate: (a) isometric view and (b) right side view



**Fig. 22** Cross-sectional micrographs of the fractured surfaces of the  $[P_{90}/P_0/F_0/P_0/P_{90}/F_{90}/P_{90}/P_0]_5$  carbon fiber composite laminate after flexural loading and (b)  $[P_{90}/P_0/F_0/P_0/P_{90}/F_{90}]$  area



### 3.3 Compression After Impact

After the CAI test, the average CAI strength of  $[P_b/F/P_b/F/P_b]_2$  carbon fiber composite laminate is 221.54 MPa, and the CAI modulus is 29.68 GPa. The average CAI strength of the autoclave process carbon fiber composite laminate is 302.68 MPa, and the CAI modulus is 33.22 GPa. Among them, since the data in the interval of 0.1–0.3% is nonlinear, the residual compression modulus is changed to the data in the interval of 0.7–1.0% for calculation. The CAI and CBI test results of the two composite laminates are shown in Table 7. Compared with the composite laminate made by the autoclave process, the residual compressive strength of this process is reduced by about 26.8%. In addition to process influence, the CAI strength was also affected by other factors, especially the fiber orientation. In previous studies by Reuda [19], they used a quasi-isotropic layup with similar thickness and showed lower CAI strength within 180 MPa. This showed that the fiber orientation had major effect in CAI testing. Moreover, Rivallant et al. [20] carried out a series of CAI tests with different impact energy (J) from 1.6 to 29.6 (J), and their result showed that the CAI strength decreased as the impact energy increased. Under the same energy (8.5 J) situation, a similar CAI strength (below 300 MPa) was obtained from their experiment, but the thickness was 4.16 mm, which was thicker than our interleaved laminate. The CAI strength is greatly affected by the fiber orientation and the layup method.

On the other hand, the average CBI strength of the  $[P_b/F/P_b]_2$  carbon fiber composite laminate is 259.43 MPa, and the CBI modulus is 30.26 GPa. The average CBI strength of the autoclave carbon fiber composite laminate is 314.08 MPa, and the CBI modulus is 33.44 GPa. Compared with the composite laminate made by the autoclave process, the CBI strength of this process is reduced by about 17.4%. In addition, the strength reduction ratio of the two composite laminates before and after impact (8.5 J) can be compared. The residual compressive strength of the composite laminate of this process after the impact is reduced by about 14.6%, while the residual compressive strength of the autoclave composite laminate after the impact is reduced by about 3.6%. The resin-rich area near the binding yarn of the dry fabric has some effect on the strength of the composites at this process.

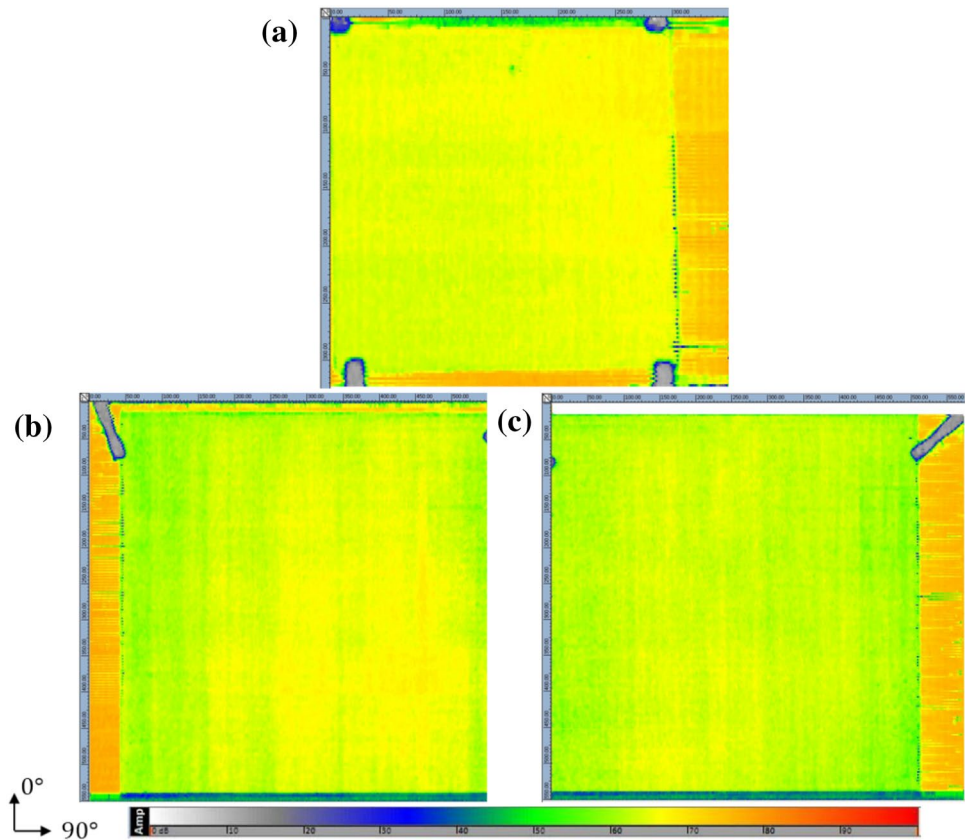
### 3.4 Composite Panel Uniformity

Figure 23 shows the ultrasonic circular SCAN (C-Scan) result of unidirectional carbon fiber composite laminates. The dark blue area in the picture is the fixture, and the fiber direction of the composite laminate is marked on the lower left, where 0 degree is along the vertical direction. The color bar reveals the echo signal strength received by the transducer, in decibels. The closer the area to the red direction, the stronger is the signal energy. The maximum value is 200 dB and the minimum value is 0 dB. Figure 23(a) shows the images of the autoclave  $30 \times 30 \text{ cm}^2$  carbon fiber

**Table 7** Comparison of CAI and CBI test data of the  $[P_b/F/P_b/F/P_b]_2$  and autoclave carbon fiber composite laminates

	CAI strength, $F^{CAI} (MPa)$	Compressive elastic modulus after impact, $E^{CAI} (GPa)$	CBI strength, $F^{CBI} (MPa)$	Compressive elastic modulus before impact, $E^{CBI} (GPa)$
$[P_b/F/P_b/F/P_b]_2$	221.54	29.68	259.43	30.26
autoclave ( $\nu_f = 0.65$ )	302.68	33.22	314.08	32.44

**Fig. 23** Ultrasonic test results: (a) autoclave process carbon fiber composite laminate, (b) Laminate A, and (c) Laminate B



composite laminate, in which the ultrasonic energy is about 160–170 dB. Figure 23(b) and (c) shows the images of the  $[P_b/F/P_b/F/P_b]_2-50 \times 50 \text{ cm}^2$  Laminate A and Laminate B, respectively. The ultrasonic energy is approximately between 150 and 165 dB. The penetration energy variation of the two detection results is very small, and no obvious pore defects are detected. In comparison, the energy variation range of this process and autoclave composite laminate is about 10–15 dB, respectively. It can be reflected that this process has low porosity quality similar to autoclave composite laminate.

For the thickness of the composites, the nine measuring points data of Laminate A and Laminate B are shown in the form of a three-dimensional histogram, reducing the range of the coordinate axis and expressed with a scale of 0.01 mm

to facilitate the observation of the difference between the measurement points. As shown in Fig. 24(A), the minimum thickness and maximum thickness of Laminate A are located at the positions of A3 (2.623 mm) and A2 (2.655 mm), respectively. The variation measure is 0.032 mm, and the standard deviation is 0.0096 mm.

As shown in Fig. 24(B), the minimum thickness and maximum thickness of Laminate B are located at the positions of C2 (2.615 mm) and A1 (2.647 mm), respectively. The maximum variation of the thickness is 0.032 mm, and the standard deviation is 0.0109 mm. It can be observed from the histogram that the thickness variation of the third row is the smallest; the thickness variation of second row is the largest. Judging from the thickness measurement results of the two composite laminates, the thickness distribution is

**Fig. 24** Three-dimensional histogram of thickness measurement data of the  $[P_b/F/P_b/F/P_b]_2-50 \times 50 \text{ cm}^2$  carbon fiber composite laminates, (a) Laminate A, and (b) Laminate B

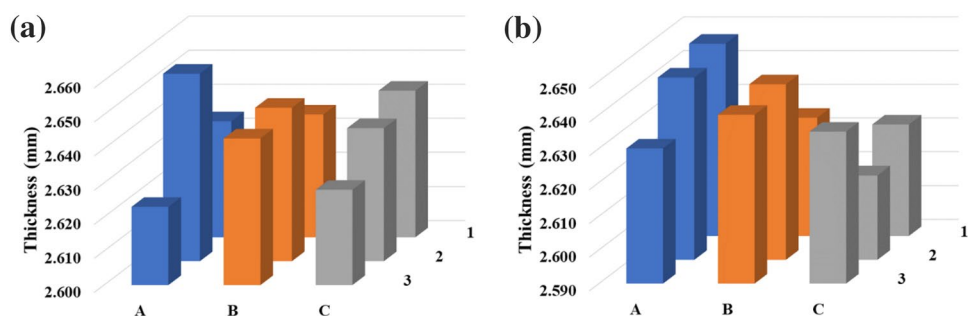


**Table 8** Statistical results of thickness measurement data of the [P<sub>w</sub>/F/P<sub>b</sub>/F/P<sub>b</sub>]<sub>2</sub>-50×50 cm<sup>2</sup> carbon fiber composite laminates

Laminate	A	B
Average (mm)	2.6384 <sup>+0.0166</sup> <sub>-0.0154</sub>	2.6334 <sup>+0.0136</sup> <sub>-0.0184</sub>
SD (mm)	0.0096	0.0109

random, and there is no trend of dimensional deviation at a specific location. As shown in Table 8, the average thicknesses of Laminate A and Laminate B are 2.6384 mm and

2.6334 mm, respectively. The difference between the two is only 0.005 mm, and the standard deviation of the two is about 0.01 mm. It can be verified that the large-size composite laminates produced by this process has good thickness uniformity and high reproducibility.

### 3.5 Woven Fiber Composites

Compression tests on the woven dry glass fabric and unidirectional glass prepreg were performed to derive the thickness variation under different compression pressures. The fitting

**Fig. 25** The thickness variation of woven glass fiber

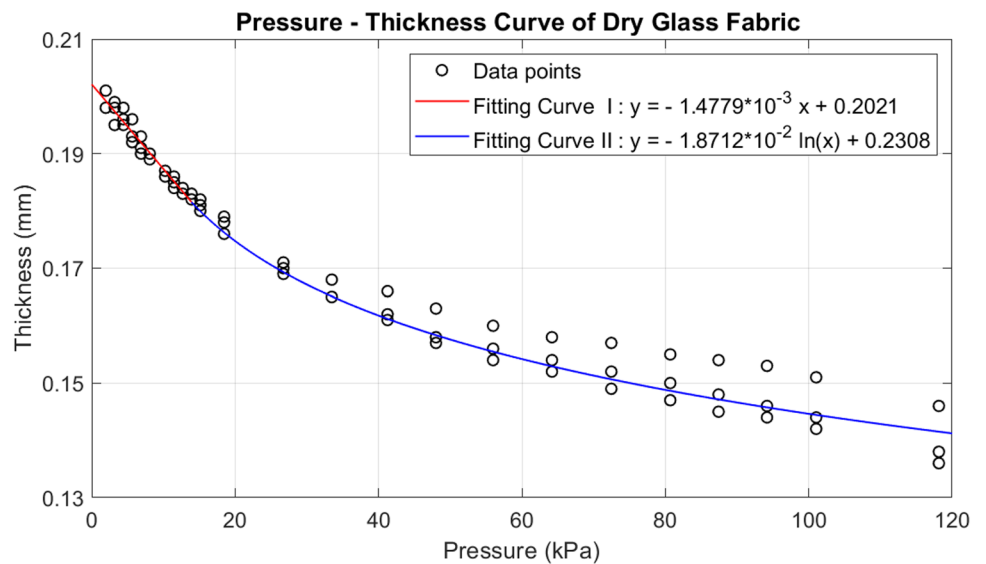


**Fig. 26** The thickness variation of glass fiber prepreg

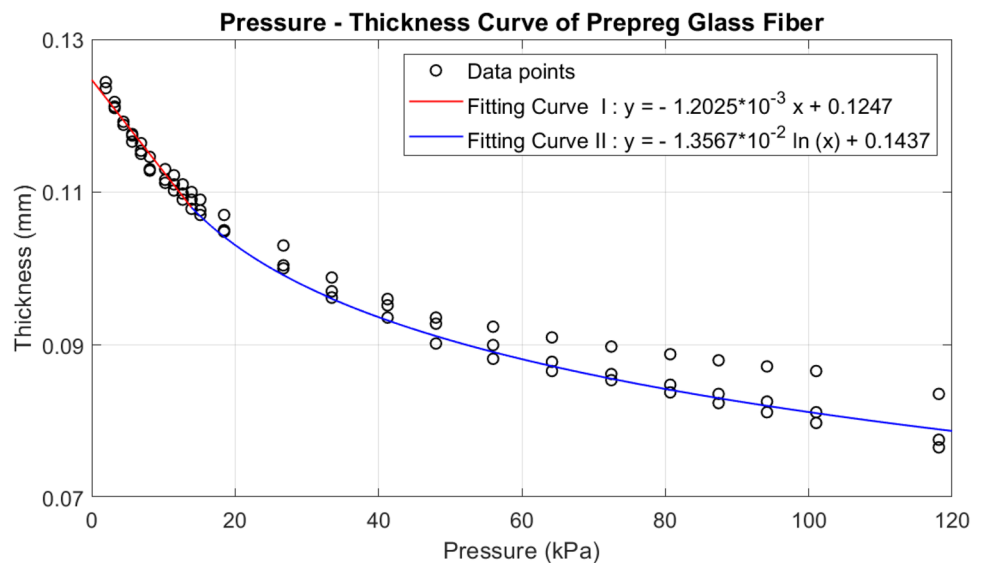
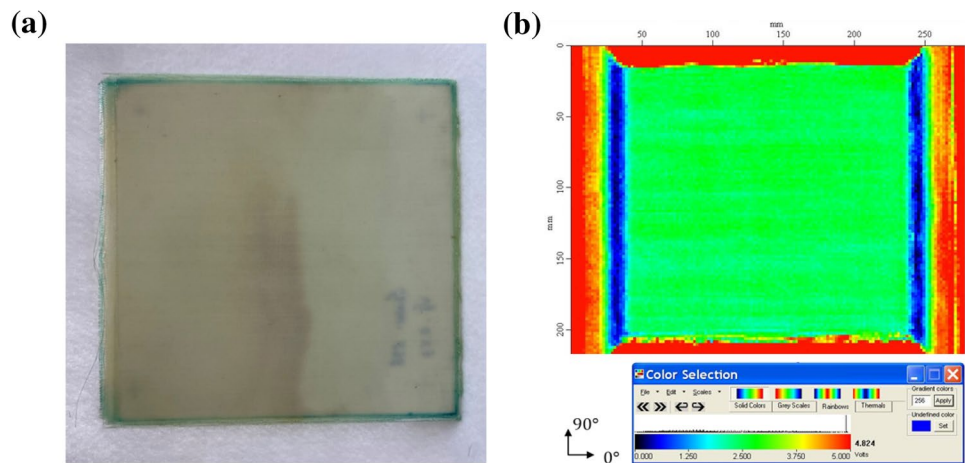




**Fig. 27** **a**  $[P_b/F/P_b/F/P_b]_2$  glass fiber composite laminate and **b** ultrasonic test result



results of the pressure–fiber thickness of the two materials are shown in Figs. 25 and 26, respectively. The pressure–fiber thickness fitting equation of the woven dry glass fabric is:

$$h_{df}^1 = -1.4779 \times 10^{-3}P + 0.2021 \quad P \leq 13.92 \text{ KPa}, \quad (5)$$

$$h_{df}^1 = -1.8712 \times 10^{-2}\ln(P) + 0.2308 \quad P > 13.92 \text{ KPa}, \quad (6)$$

where  $h_{df}^1$  is the thickness of one layer dry fiber in the unit of mm and  $P$  is the fiber pressure in the unit of (KPa). The pressure–fiber thickness fitting equation of the unidirectional glass prepreg is:

$$h_{pf}^1 = -1.2025 \times 10^{-3}P + 0.1247 \quad P \leq 13.92 \text{ KPa}, \quad (7)$$

$$h_{pf}^1 = -1.3567 \times 10^{-2}\ln(P) + 0.1437 \quad P > 13.92 \text{ KPa}, \quad (8)$$

where  $h_{pf}^1$  is the thickness of one layer prepreg in the unit of mm.

After the calculation of the saturation index in the laminate, we also choose the  $[P_b/F/P_b/F/P_b]_2$  layup to make the glass fiber composite laminate. The finished composite laminate is shown in Fig. 27(a), where the saturation index  $S_{\text{index}} = 1.83$  and the fiber volume ratio  $v_f = 0.53$ . Figure 27(b) is the scanning result of C-Scan, and the fiber direction of the composite laminate is marked on the lower left. The color bar above is the intensity of the signal received by the transducer, and the unit is volts. The closer the area to the red direction, the stronger is the signal energy. The detection result is uniform green and the signal intensity is about 1.875–3.125 volts. No obvious defect color is detected. It reflects the feasibility of the process to produce laminates of different materials or woven forms.

## 4 Conclusion

In this study, the vacuum-bag-only process was used to fabricate composite laminates by employing interleaved unidirectional fully impregnated prepreg and dry fiber.

1. The mechanical properties test results show that the flexure strength, CAI strength and CBI strength of the carbon fiber composite laminate of this process are about 84%, 72% and 83% of the autoclave composite laminate, respectively.
2. After FIB microstructure analysis, it is shown that the main reason for the weaker strength of the composite laminate in this process is caused by the weaving “weft” of the unidirectional carbon fiber dry fabric, which may result in resin-rich area or voids. Therefore, when the composite laminate was bent or compressed, the interface between the carbon fiber dry fabric and the prepreg cloth is prone to delamination.
3. In the bidirectional composites, the layup sequence may have some effect on the void formation near the weft binding yarns.
4. The interleave prepreg and dry fabric composites made by the VBO process shows good uniformity and repeatability. The mechanical properties in terms of bending strength and CAI are less than those by the autoclave process. However, about 80% strength can be achieved for the composites by this VBO process.

**Acknowledgements** The authors would like to thank the financial support from Ministry of Science and Technology in Taiwan under the contract number of MOST 109-2221-E-006-030. In addition, the authors would like to thank the assistance from the Aeronautical Systems Research Division of National Chung-Shan Institute of Science and Technology (NCSIST) in Taiwan, for the successful completion of the ultrasonic detection part of this paper.

**Data availability statement** The datasets generated during and/or analysed during the current study are available from the corresponding author on reasonable request.

## Declarations

**Conflict of interest** The authors declare no conflict of interest.

## References

1. F. C. Campbell Jr, Manufacturing technology for aerospace structural materials, Elsevier, (2011)
2. L. Grunenfelder, T. Centea, P. Hubert, S. Nutt, *Compos. A Appl. Sci. Manuf.* **45**, 119 (2013)
3. T. Centea, S. Hughes, S. Payette, J. Kratz, and P. Hubert, in "53rd AIAA/ASME/ASCE/AHS/ASC Structures, Structural Dynamics and Materials Conference 20th AIAA/ASME/AHS Adaptive Structures Conference 14th AIAA"Ed.^Eds.), 1568, Year of Convergence.
4. T. Centea, L.K. Grunenfelder, S.R. Nutt, *Compos. A Appl. Sci. Manuf.* **70**, 132 (2015)
5. R. Harshe, *J. Indian Inst. Sci.* **95**, 207 (2015)
6. S.Y. Park, C.H. Choi, W.J. Choi, S.S. Hwang, *Appl. Compos. Mater.* **26**, 187 (2019)
7. S. M. Hughes and P. Hubert, *SAMPE Tech*, (2013).
8. Y.-H. Yang, W.-B. Young, *Fibers Polym.* **22**, 460 (2021)
9. M. S. Moreno, A. R. Gutierrez, and J. M. Vicente, in "IOP Conference Series: Materials Science and Engineering"Ed.^Eds.), 012047, Year of Convergence.
10. I. ASTM, ASTM D790-07, (2007).
11. M. Richardson, M. Wisheart, *Compos. A Appl. Sci. Manuf.* **27**, 1123 (1996)
12. A. Amaro, P. Reis, M. De Moura, *Strain* **47**, 203 (2011)
13. S. Sanchez-Saez, E. Barbero, R. Zaera, C. Navarro, *Compos. Sci. Technol.* **65**, 1911 (2005)
14. A. International, "Standard test method for measuring the damage resistance of a fiber-reinforced polymer matrix composite to a drop-weight impact event", ASTM International, (2007)
15. A. Standard, *ASTM D7137/D7137M* (American Society for Testing and Materials, West Conshohocken, 2007)
16. A. Stamopoulos, K. Tserpes, P. Prucha, D. Vavrik, *J. Compos. Mater.* **50**, 2087 (2016)
17. Y. Mujahid, N. Sallih, M.Z. Abdullah, M. Mustapha, *Polym. Compos.* **42**, 567 (2021)
18. M. Pishvar, M. Amirkhosravi, M.C. Altan, *Polym. Compos.* **40**, 159 (2019)
19. S. H. Rueda, Curing, defects and mechanical performance of fiber-reinforced composites, Universidad Politécnica de Madrid, (2013)
20. S. Rivallant, C. Bouvet, E. Abi Abdallah, B. Broll, and J.-J. Barrau, *Composite Structures*, **111**, 147 (2014)
21. P. Hubert, T. Centea, L. Grunenfelder, S. Nutt, J. Kratz, and A. Lévy, *2.4 Out-of-Autoclave Prepreg Processing*, Elsevier, (2018)

Springer Nature or its licensor (e.g. a society or other partner) holds exclusive rights to this article under a publishing agreement with the author(s) or other rightsholder(s); author self-archiving of the accepted manuscript version of this article is solely governed by the terms of such publishing agreement and applicable law.